Available online at www.sciencedirect.com
ScienceDirect
Trans. Nonferrous Met. Soc. China 24(2014) 3076−3083
Transactions of Nonferrous Metals Society of China
www.tnmsc.cn

Precipitation kinetics of 2519A aluminum alloy based on aging curves and DSC analysis

Yi-ping WU[1], Ling-ying YE[1], Yu-zhen JIA[2], Ling LIU[3], Xin-ming ZHANG[1]

1. School of Materials Science and Engineering, Central South University, Changsha 410083, China;
2. Bichamp Cutting Technology (Hunan) Co., Ltd., Changsha 410200, China;
3. Parametric Technology Corporation, Shanghai 200120, China

Received 20 August 2013; accepted 24 December 2013

Abstract: The precipitation kinetics of 2519A aluminum alloy after different cold rolling reductions before aging was investigated by hardness test and differential scanning calorimetry (DSC). The activation energy was calculated according to DSC curves using single heating rate method. The microstructures of as-rolled and peak-aged alloys were observed by transmission electron microscopy (TEM). The result shows that the age hardenability reduces and the activation energy rises with increasing the reduction from 7% to 40%. Nonuniform dislocations are found in as-rolled alloy and inhomogeneous distribution of θ' phase is revealed in peak-aged alloy when the reduction is 15%. The inhomogeneous distribution of θ' phase may be related to the age hardenability reducing and activation energy rising.

Key words: 2519A aluminum alloy; dislocation structure; precipitation kinetics; θ' phase; differential scanning calorimetry (DSC)

1 Introduction

The 2519 alloy is a kind of aluminum alloy with high strength and corrosion cracking resistance. It was developed by Aluminum Company of America in 1980s [1]. Nowadays, it has been applied for aircraft, helicopters and the advanced amphibious assault vehicle (AAAV) to lighten the mass for its low density [1,2]. 2519A aluminum alloy, developed based on 2519 aluminum alloy, exhibits higher strength and good ballistic performance because of fine distribution of θ' [3−5].

It is well known that precipitation is strongly related to cold working between quenching and aging in age-hardenable aluminum alloys. In general, the formation of semi-coherent θ' in 2000 series aluminum alloy can be promoted by appropriate cold working before aging by introducing dislocations during cold working, because dislocations can lower the energy barrier and stimulate the formation of θ', although the formation of GP zone is suppressed. However, the formation of semi-coherent Ω phase in Al−Cu−Mg−Ag quaternary alloy is restrained by cold work [6,7]. Furthermore, ZHOU et al [8] found that increasing deformation amount negatively affects the mechanical properties of Al−Cu−Li−Sc alloy when the pre-stretching amount is larger than 5.6% due to the inhomogeneous distribution of semi-coherent T1 phase. It is also found that the yield strength of 2519A aluminum alloy decreases when the rolling reduction increases from 10% to 25% before aging [9]. LIU [10] proposed that when the rolling reduction is up to 90%, θ' is found in low-density dislocation area rather than in high-density one, resulting in the slight increase of hardness at the beginning of aging followed by sharp decrease. Similar result was found in severely deformed specimen of aged 6022 alloy [11].

It can be seen that the relationship between cold work amount and precipitations is complicated. Revealing the relationship between θ' and pre-deformation needs further understanding on the process of precipitation, for example, by studying precipitation kinetics. However, most of the attention was paid to the ultimate property like hardness and strength of peak-aged state on age-hardenable aluminum alloy up to the present. Few researches were reported on the precipitation kinetics.

Foundation item: Project (2012CB619500) supported by the National Basic Research Program of China
Corresponding author: Ling-ying YE; Tel: +86-731-88830265; E-mail: yelingying_1981@163.com
DOI: 10.1016/S1003-6326(14)63445-2

In this work, the influence of cold rolling reduction on precipitation kinetics was studied, the aging hardening behavior and activation energy were characterized, and the related mechanisms were discussed.

2 Experimental

The nominal composition of 2519A aluminum alloy is listed in Table 1. The 60 mm thick aged plate was re-dissolved at 808 K for 6 h, and then quenched into room temperature water immediately. The as-quenched plates were cold-rolled by 7%, 15%, 30% and 40% reduction, respectively, and then aged at 438 K for different time. In order to avoid that the results were affected by some factors, all the samples were cut from the center layer of the plates.

Table 1 Chemical compositions of 2519A aluminum alloy (mass fraction, %)

Cu	Mg	Mn	Zr	Fe	Si	Al
5.80	0.20	0.30	0.20	0.20	0.10	Bal.

The hardness tests were performed on HV-10B with 29.4 N load. DSC measurements of as-rolled samples were carried out at a heating rate of 10 K/min by the NETZSCH DSC 200 F3 thermal analyzer. Microstructure characterizations were observed with transmission electron microscope (TEM, Tecnai G^2 20) operated at 200 kV. The disk specimens for TEM were cut from the plate along the rolling direction. They were ground down to about 60 μm, and then electro-polished in a 3:7 HNO_3−CH_3OH solution at about 250 K in a twin-jet electro-poling unit.

3 Results and discussion

3.1 Aging hardening behavior

Figure 1 shows the Vickers hardness curves of 2519A alloy aged at 438 K with different reduction rates. It can be seen that the hardness of as-rolled state increases from HV123 to HV148 with increasing the reduction from 7% to 40%, which is caused by the strain hardening. The time to the peak age of each alloy is within 5 h, which is quite short compared to former research [4,12]. This result is interesting and further work is intended to be done and fill this gap. The time to the peak ageing is slightly shortened from 5 to 4 h with increasing reduction from 7% to 40%, while the hardness in peak-aged state decreases with reduction increasing from 7% to 15%, and increases from 15% to 40%. Recovery may occur in 2519A aluminum alloy at 438 K, but the movement of dislocation will be blocked by the precipitation [13,14]. Therefore, the hardness in peak-aged state is composed of matrix hardness, precipitation hardening and strain hardening. Since recovery is blocked by the precipitation, and the variation of solid solution doesn't result in large change of matrix hardness, the aging hardening is mainly caused by the precipitation. Therefore, parameters ΔH is introduced to define the age hardenability in this work, which is listed in Table 2. A quick decrease of ΔH is observed with increasing reduction from 7% to 30%, while ΔH increases a little when reduction changes from 30% to 40%. It can be seen that the age hardenability is weakened with increasing reduction from 7% to 40%.

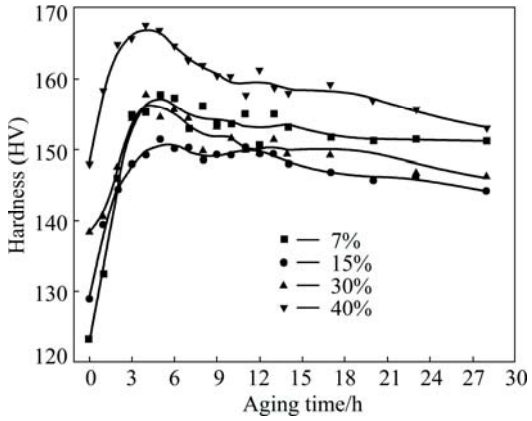

Fig. 1 Vickers hardness curves of 2519A alloy aged at 438 K with different reduction rates

Table 2 Vickers hardness of 2519 alloy with different reduction rates

Reduction	Peak-aged time/h	Hardness of as-rolled samples, H_{ar}	Hardness of peak-aged samples, H_{pa}	Increase in hardness, $\Delta H=H_{pa}-H_{ar}$
7%	5	123	158	35
15%	5	129	152	23
30%	4	138	158	20
40%	4	148	167	19

In fact, similar results can be obtained in previous study. The data of related references listed in Table 3 were collected, which agrees to the result of this work. Although a certain pre-deformation amount enhances the hardness of peak-aged alloys due to the fine and disperse precipitates, the hardness difference decreases significantly, proving the weakening of age hardenability by pre-deformation in all the alloys, as listed in Table 3, compared to the undeformed alloys (except that for AA2524 alloy, 2% pre-deformation increases the hardness difference compared to the undeformed alloy. However, with increasing pre-deformation from 2% to 5%, the hardness difference decreases again).

3.2 DSC analysis and activation energy determination

The DSC curves of different reduction samples are shown in Fig. 2. In each curve, there is a major peak

Table 3 Hardness difference between as-deformed and peak-aged alloys in references

Alloy	Aging temperature/°C	Deformation amount/%	Hardness		Hardness difference
			As-deformed alloy	Peak-aged alloy	
Al−5Cu−0.5Mg [7]	200	0	44 (HRB)	76 (HRB)	32 (HRB)
		6	58 (HRB)	81 (HRB)	23 (HRB)
Al−4Cu−0.3Mg [6]	190	0	84 (VHN)	130 (VHN)	46 (VHN)
		6	99 (VHN)	137 (VHN)	38 (VHN)
AA2618 [15]	200	0	77 (HBS)	148 (HRS)	71 (HRS)
		10	135 (HBS)	159 (HBS)	24 (HRS)
AA2524 [16]	170	0	97 (VHN)	142 (VHN)	45 (VHN)
		2	108 (VHN)	163 (VHN)	55 (VHN)
		5	125 (VHN)	170 (VHN)	45 (VHN)
Al−2.6Cu−1.3Mg [17]	170	0	34.2 (HRB)	69 (HRB)	34.8 (HRB)
		1.5	43 (HRB)	71.8 (HRB)	28.8 (HRB)
AA2024 [17]	170	0	53 (HRB)	78 (HRB)	25 (HRB)
		1.5	60 (HRB)	82 (HRB)	22 (HRB)

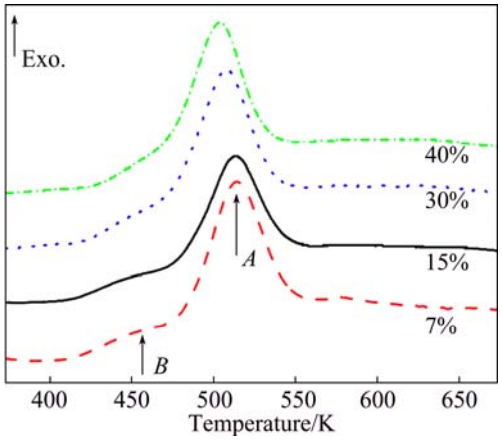

Fig. 2 DSC curves of as-rolled 2519A aluminum alloy after different cold-rolling reductions

(marked by arrow *A*), which is due to the nucleation and growth of semi-coherent θ' [18]. The temperature of the peak *A* decreases with increasing the reduction. The peak temperature of the sample subjected to 7% cold rolling is 514 K, while that of the sample subjected to 40% decreases to 503 K. There is a tiny peak attaching to the major peak *A* on each curve (marked by arrow *B*), which becomes weak with increasing the cold rolling reduction, and it is hardly found on the curve of the sample after 40% reduction. This peak may be related to the formation of coherent GP zone or phase θ'' [12].

A single heating-rate expression is used to calculate the activation energy [19,20]:

$$\ln\left(\frac{\mathrm{d}y}{\mathrm{d}T}\frac{\Phi}{f(y)}\right)=\ln k_0-\frac{Q}{R}\left(\frac{1}{T}\right) \tag{1}$$

where T is Kelvin temperature; y is the transformation fraction of peak *A* on DSC curves in Fig. 2, $0<y<1$; Φ is the heating rate, which is 10 K/min in this study; Q is the activation energy; k_0 is a constant; R is the mole gas constant; $f(y)$ is the reaction function, which is to be selected. According to JMA model, $f(y)$ can be expressed as [21]

$$f(y)=n[-\ln(1-y)]^{\frac{n-1}{n}}(1-y) \tag{2}$$

where n gives a straight line of Eq. (2). Therefore, if $\ln[(\mathrm{d}y/\mathrm{d}T)(\Phi/f(y))]$ versus $1/T$ is plotted and fits a line, the activation energy can be determined by the slope. According to Ref. [21], n corresponds to the mechanism of nucleation and growth of phase. In order to determine n, 0.5, 1, 1.5, 2, 2.5 and 3 are tried as the value of n to fit the $\ln[(\mathrm{d}y/\mathrm{d}T)(\Phi/f(y))]$ versus $1/T$ line, as well as $(1-y)^{1/2}$, $(1-y)^{2/3}$, $y^{1/3}(1-y)$ and 1 as the expression of $f(y)$ [21]. The best fitting line is obtained with $f(y)=y^{1/3}(1-y)$. Be aware that expression of $f(y)$ shows the precipitation mechanism, which is controlled by precipitate growth in three-dimensions after saturation of nucleation in mean field approximation with $f(y)=y^{1/3}(1-y)$ [21]. As plate-shape phase, θ' grows in radius direction at first, and then in normal direction to transform to non-coherent θ finally. In other word, when θ' grows in three-dimensions, it starts to transform to θ.

Figure 3 shows the results of plots and fitting lines on Eq. (1) for various reductions at different values of y (0.05, 0.20, 0.35, 0.50, 0.65, 0.80 and 0.95) by $f(y)=y^{1/3}(1-y)$. The values of Q are listed in Table 4, determined by the slope of the fitting lines. Surprising, the activation energy of the alloy goes up from 106.5 kJ/mol to 114.6 kJ/mol when the plate is cold-rolled by reduction from 7% to 30%, while it rises slightly with increasing reduction from 30% to 40% (only from 114.6 kJ/mol to 114.8 kJ/mol), although the peak temperature decreases. The result meets the change of hardness difference.

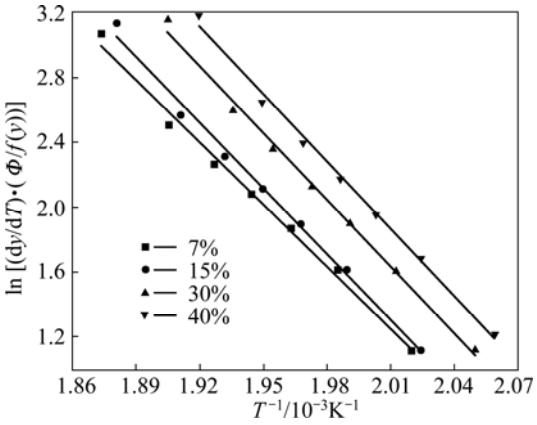

Fig. 3 Fitting lines of calculated activation energies of θ' phase in 2519A aluminum alloy

Table 4 Kinetic parameter values for θ' formation in 2519A aluminum alloy

Reduction	Peak temperature/K	Activation energy/ (kJ·mol^{-1})
7%	514	106.5
15%	513	112.6
30%	508	114.6
40%	504	114.8

Effect of cold rolling on precipitation has been researched for decades. It was put forward that θ' formation was affected positively by appropriate cold work. The previous investigation shows that both 6% stretching and rolling before aging accelerate and promote the formation of θ' by introducing dislocations, where θ' precipitates preferentially, providing a large amount of nucleating positions [6,7]. However, the deformation amount in Refs. [6,7] is 6%, not referring to the larger deformation. In this research, the reduction is from 7% to 40%, and the result shows that larger deformation suppresses the θ' precipitation and growth according to the increasing of activation energy and decreasing of hardness difference, as shown in Fig. 4(a). Interestingly, activation energy shows a linear relationship with hardness difference, which needs further research to deep into it.

The data collected above indicate that the mechanism of the effect of larger cold rolling on the θ' phase may be distinguished from that of lower cold rolling.

3.3 Precipitation in alloy

Since 2519A aluminum alloy plate is mainly strengthened by precipitation of θ', large attention is focused on the distribution of θ'. Representative microstructures of as-rolled and peak-aged plates are shown in Fig. 5. Two distinguished zones are found in

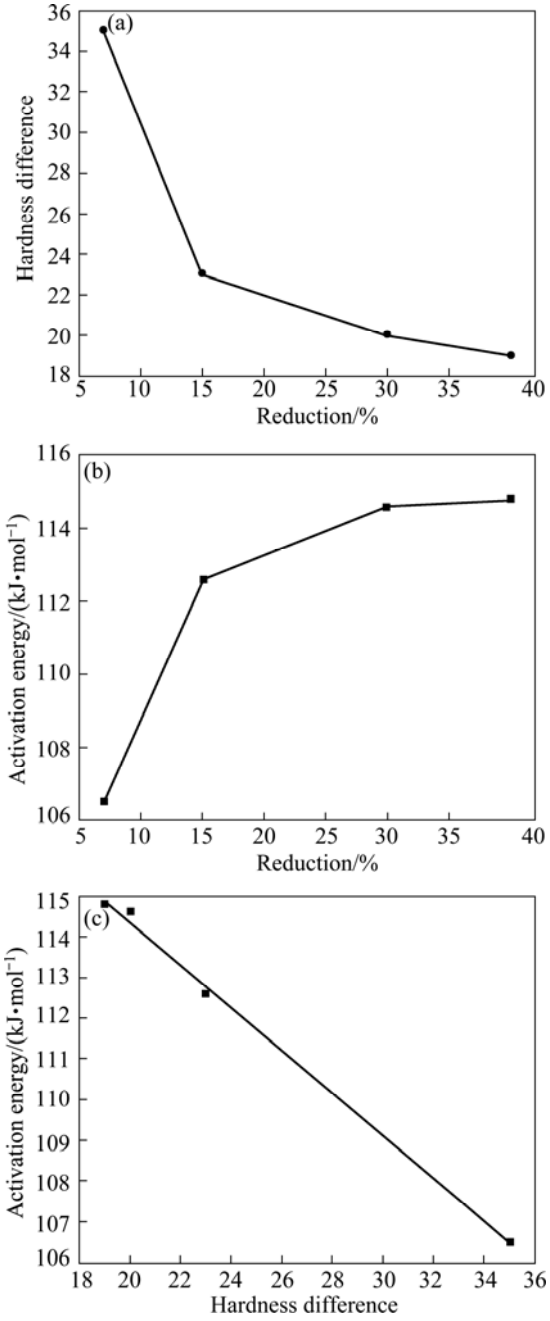

Fig. 4 Relationships between hardness difference and reduction (a), activation energy and reduction (b) and activation energy and hardness difference (c)

the microstructure in as-rolled plates: low density dislocation zone (LDDZ) and high density dislocation zone (HDDZ), as shown in Fig. 5(a). Since dislocations are the preferable positions for θ' to nucleate, nonuniform dislocations are easy to form inhomogeneous θ', as shown in Figs. 5(b) and (c). It is found that thick θ' distributes in areas both near grain boundary and in grain interior, which are plausible to be the original HDDZ in as-rolled state, and beside the areas θ' is relatively thin (arrowed in Figs. 5(b) and (c)). However, homogeneous θ' is found when reduction is

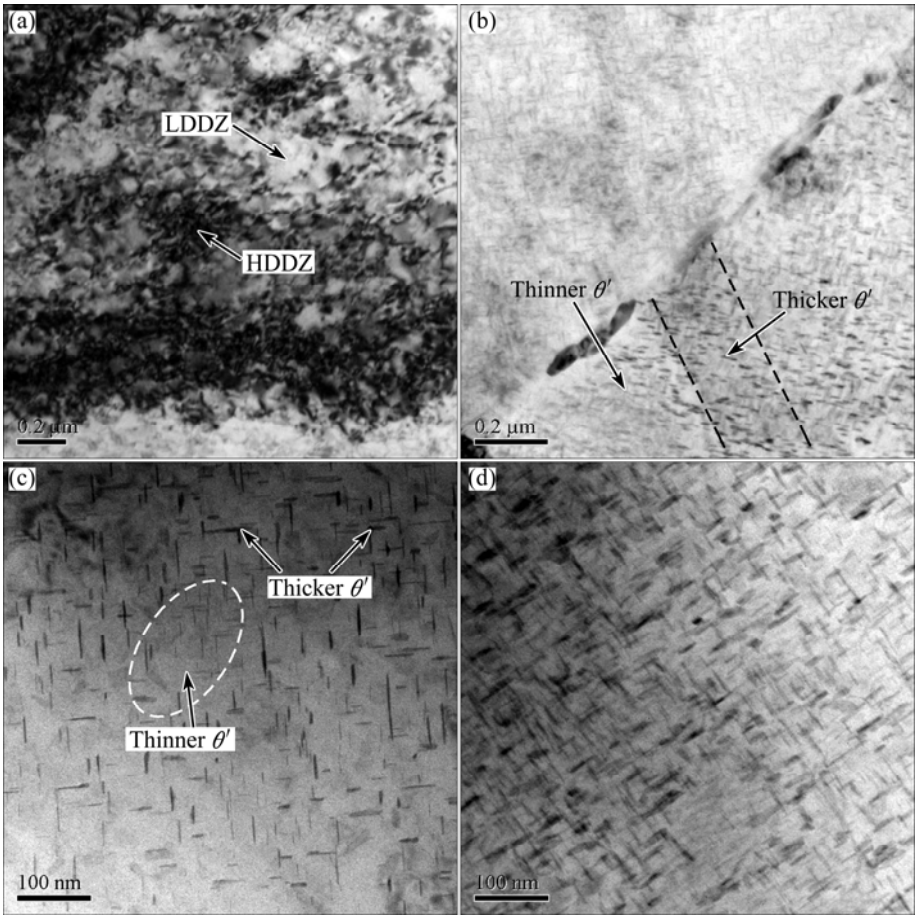

Fig. 5 Microstructures of 2519A aluminum alloys as-rolled with 15% reduction rate (a), peak-aged with 15% reduction rate, near grain boundary (b), peak-aged with 15% reduction rate, in grain interior (c) and peak-aged with 7% reduction rate (d)

7%, as shown in Fig. 5(d). It is worth emphasizing that hardness difference decreases while activation energy raises a lot with increasing reduction from 7% to 15%, which may be related to inhomogeneous distribution of θ'.

Two mechanisms has been promoted to explain the formation of θ': 1) Altering based on coherent θ'' [22]. When the dislocation density is very low, Cu atoms have to gather together through diffusing, forming coherent phase and then growing to semi-coherent θ'; 2) Precipitating along dislocations [6]. If there are dense dislocations in the matrix, θ' can nucleate along dislocations rather than be altered from coherent phase. The density of dislocation in the alloy after cold work is surely higher than that in the as-quenched alloy. Therefore, in as-rolled alloy, the formation of θ' depends on the dislocation structure which relates to the rolling reduction. However, different deformation amounts correspond to different dislocation appearances [13]. Relatively disperse dislocation is obtained by appropriate deformation due to the difficult moving of dislocations at this condition, while the dislocation cell is formed with increasing the deformation to a certain level, because the mobile dislocations interact with each other and divide volume into several cells [8,23]. The dislocation density on cell boundary is much larger than that in cell interior. The cell boundary is a kind of typical HDDZ, while cell interior is a type of LDDZ. In this work, distinguished dislocation zones, HDDZ and LDDZ, can be found when reduction is 15%, as shown in Fig. 5(a). Actually, this featured microstructure is proved to be present in the alloys after a certain amount of deformation, e.g. pure Al after 5% cold deformation [13] and as-quenched Al−Mg−Si alloy after 80% cold rolling [24]. In this work, the microstructure is featured in the as-quenched 2519A alloy after 15% cold rolling. Since the semi-coherent θ' prefers to precipitate along dislocations, homogeneous θ' forms in the microstructure with disperse dislocations (Fig. 6(a)), while the nonuniform dislocation results in the inhomogeneous distribution of θ' (Fig. 6(b)). There is less precipitates in the LDDZ for the much sparser dislocation and fewer Cu atoms diffusing to the area because most atoms diffuse to the HDDZ. Therefore, the precipitates disperse inhomogeneously, thicker and denser in HDDZ, and thinner and sparser in LDDZ, and this kind of microstructure is observed by TEM observation in the peak-aged alloys after 15% reduction, as shown in Figs. 5(b) and (c).

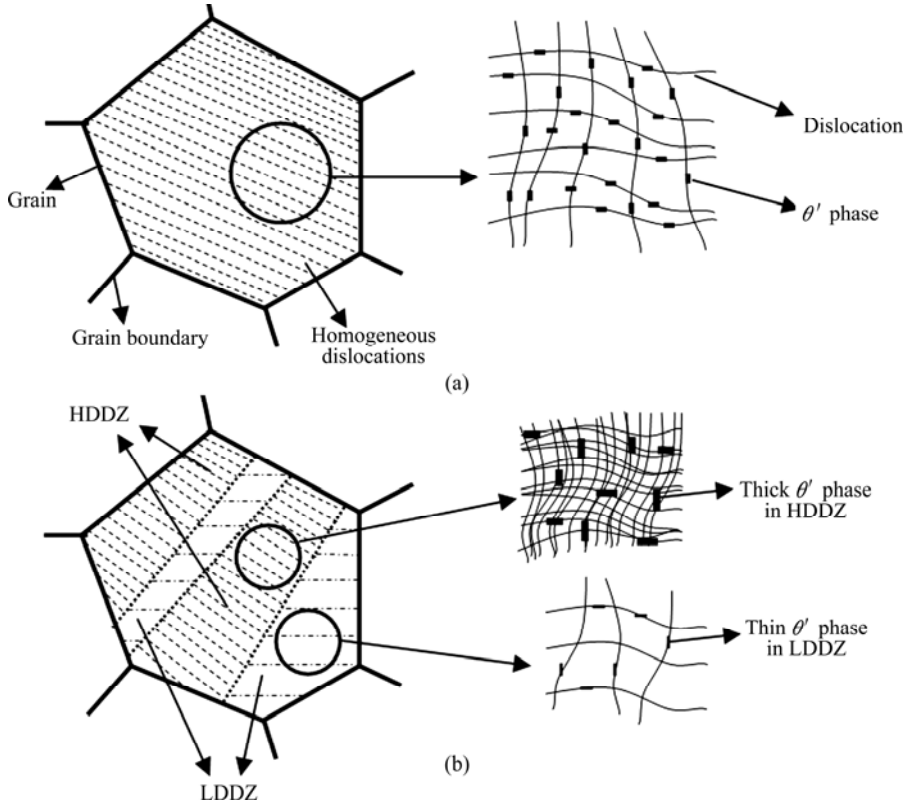

Fig. 6 Schematics of microstructures of peak-aged 2519A aluminum alloy: (a) Formation of homogeneous dislocation structure; (b) Formation of nonuniform dislocation structure

Although LDDZ forms with increasing the reduction, it is plausible that the average density of dislocation increases. Therefore, it is easier for Cu atoms to diffuse. Since formation of θ' depends on the diffusion of Cu atoms, it may be beneficial for θ' to nucleate macroscopically, resulting in the decrease of temperature of peak A on DSC curves and shortening of peak-aged time with increasing reduction from 7% to 40%. However, problems may be brought in by inhomogeneous dislocation structure. First, since Cu atoms prefer to diffuse along HDDZ, the area for θ' to nucleate and grow up decreases. Second, θ' phases with the habit plane of {001}[25−27] block each other to grow up. For example, there are two vertical edge dislocations close to each other, as shown in Fig. 7(a). Cu atoms diffuse along both dislocations and gather together to form clusters (Fig. 7(b)). With more atoms diffusing to the area, two nuclei of θ' form (Fig. 7(c)). Because these two nuclei are perpendicular to each other in this condition, they may stop growing if the stored energy is not enough, or grow at both radius and thickness direction, forming non-coherent θ when enough stored energy is obtained. As mentioned in Section 3.2, the expression of $f(y)=y^{1/3}(1-y)$ to give the best fitting line hints the precipitation mechanism controlled by precipitate growth in three dimensions. It is

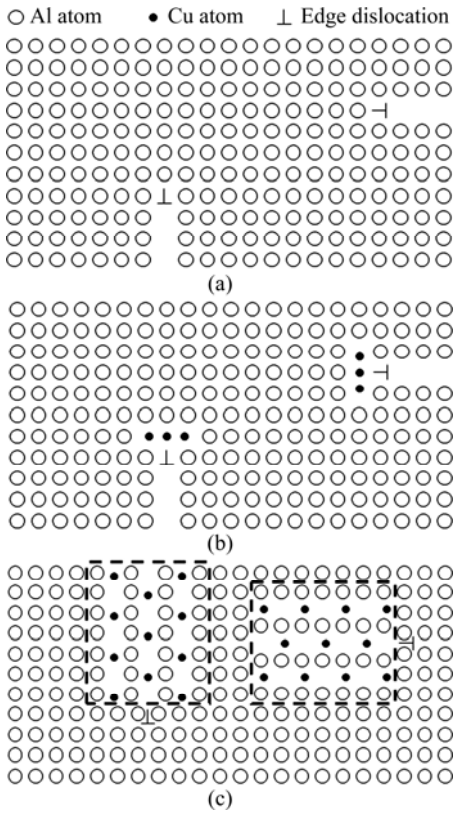

Fig. 7 Schematics of ways that dislocations affect growth of θ': (a) Two vertical edge dislocations; (b) Cu atoms diffusing with dislocations; (c) Formation of perpendicular θ' particles

believed that in this work the latter situation happens in HDDZ, resulting in the consuming of large stored energy to form the thick θ'. This may be the reason why the activation energy rises with increasing reduction. However, the effects of cold work on precipitation kinetics in age-hardenable aluminum alloys are needed to be clarified.

4 Conclusions

1) The age hardenability reduces with increasing the reduction rate from 7% to 30%. The age hardenability will increase when the reduction rate increases from 30% to 40%. This is proved by the decreasing of hardness difference between peak-aged state and as-rolled state and the increasing of activation energy of θ' phase growth.

2) Inhomogeneous distribution of θ' phase is found when the reduction is 15%, while θ' phases are relatively homogeneous when the reduction is 7%. Inhomogeneous distribution of θ' phase may be related to the weakening of age hardenability.

References

[1] SANDERS R E Jr, PETIT J I. High strength weldable aluminum base alloy product and method of making same: US, 4610733[P]. 1986−09−09.

[2] FISHER J J Jr, KRAMER L S, PICHENS J R. Aluminum alloy 2519 in military vehicles [J]. Advance Materials and Processing, 2002, 160(9): 43−46.

[3] ZHANG Xin-ming, LIU Ling, YE Ling-ying, LIU Jun, LEI Zhao, SONG Ji-chao. Effect of pre-deformation of rolling combined with stretching on stress corrosion of aluminum alloy 2519A plate [J]. Transactions of Nonferrous Metals Society of China, 2012, 22(1): 8−15.

[4] ZHANG Xin-ming, WANG Wen-tao, CHEN Ming-an, GAO Zhi-guo, JIA Yu-zhen,YE-Ling-ying, ZHENG Da-wei, LIU Ling, KUANG Xiao-yue. Effects of Yb addition on microstructures and mechanical properties of 2519A aluminum alloy plate [J]. Transactions of Nonferrous Metals Society of China, 2010, 20(5): 727−731.

[5] ZHANG Xin-ming, LI Hui-jie, LI Hui-zhong, GAO Hui, GAO Zhi-guo, LIU Ying, LIU Bo. Dynamic property evaluation of aluminum alloy 2519A by split Hopkinson pressure bar [J]. Transactions of Nonferrous Metals Society of China, 2008, 18(1): 1−5.

[6] RINGER S P, MUDDLE B C, POLMEAR I J. Effects of cold work on precipitation in Al−Cu−Mg−(Ag) and Al−Cu−Li−(Mg−Ag) alloys [J]. Metallurgical and Materials Transactions A, 1995, 26(7): 1659−1671.

[7] ÜNLÜ N, GABLE B M, SHIFLET G J, STARKE E A Jr. The effect of cold work on the precipitation of Ω and θ' in a trenary Al−Cu−Mg alloy [J]. Metallurgical and Materials Transactions A, 2003, 34(12): 2757−2769.

[8] ZHOU Chang-rong, LIU Xin-yu, PAN Qing-lin. Effect of pretension on microstructure and tensile property of Al−Cu−Li alloy containing Scandium [J]. Chinese Journal of Rare Metals, 2005, 29(6): 837−840. (in Chinese)

[9] ZHANG Xin-ming, LIU Ling, JIA Yu-zhen. Effects of stretching and rolling pre-deformation on microstructures and mechanical properties of 2519A aluminum alloy [J]. The Chinese Journal of Nonferrous Metals, 2010, 20(6): 1088−1094. (in Chinese)

[10] LIU Ying. Effects of thermomechanical heat treatment on microstructure, mechanical properties and corrosion resistance of 2519A aluminum alloy [D]. Changsha: Central South University, 2008: 52−68. (in Chinese)

[11] HIROSAWA S, HAMAOKA T, HORITA Z, LEE S, MATSUDA K, TERADA D. Methods for designing concurrently strengthened severely deformed age-hardenable aluminum alloys by ultrafine-grained and precipitation hardenings [J]. Metallurgical and Materials Transactions A, 2013, 44(8): 3921−3933.

[12] WANG Wen-tao, ZHANG Xin-ming, GAO Zhi-guo, JIA Yu-zhen, YE Ling-ying, ZHENG Da-wei, LIU Ling. Influence of Ce addition on the microstructures and mechanical peroperties of 2519A aluminum alloy plate [J]. Journal of Alloys and Compounds, 2010, 491(1−2): 366−371.

[13] ZLATEVA G, MARTINOVA Z. Microstructure of metals and alloys—An atlas of transmission electron microscopy images [M]. New York: CRC Press, 2008: 93−96.

[14] HUMPHREYS F J, HATHERLY M. Recrystallization and related annealing phenomena [M]. Oxford: Elsevier, 2004: 207−213.

[15] WANG Jian-hua, YI Dan-qing, SU Xu-ping, YIN Fu-cheng. Influence of deformation ageing treatment on microstructure and properties of aluminum alloy 2618 [J]. Materials Characterization, 2008, 59(7): 965−968.

[16] QUAN Li-wei, ZHAO Gang, GAO S, MUDDLE B C. Effect of pre-stretching on microstructure of aged 2524 aluminium alloy [J]. Transactions of Nonferrous Metals Society of China, 2011, 21(9): 1957−1962.

[17] SHIH H C, HO N J, HUANG J C. Precipitation behaviors in Al−Cu−Mg and 2024 aluminum alloys [J]. Metallurgical and Materials Transactions A, 1996, 27(9): 2479−2494.

[18] RIONTINO G, MARTINZ H P, MENGUCCI P. DSC investigation of natural ageing in high-copper AlCuMg alloys [J]. Materials Science Forum, 2000, 331: 1025−1030.

[19] LUO A, LLOYD D J, GUPTA A K, YOUDELIS W V. Precipitation and dissolution kinetics in Al−Li−Cu−Mg alloy 8090 [J]. Acta Metallurgica et Materialia, 1993, 41(3): 769−776.

[20] JENA A K, GUPTAA K, CHATURVEDI M C. A differential scanning calorimetric investigation of precipitation kinetics in the Al−1.53wt%Cu−0.79wt%Mg alloy [J]. Acta Metallurgica, 1989, 37(3): 885−895.

[21] STARINK M J. Analysis of aluminium based alloys by calorimetry: quantitative analysis of reactions and reaction kinetics [J]. International Materials Reviews, 2004, 49(3−4): 191−226.

[22] SON S K, TAKEDA M, MITOME M, BANDO Y, ENDO T. Precipitation behavior of an Al−Cu alloy during isothermal aging at low temperatures [J]. Materials Letters, 2005, 59(6): 629−632.

[23] YUAN Zhi-shan, LU Zheng, XIE You-hua, DAI Sheng-long, LIU Chang-sheng. Effect of plastic deformation on microstructure and properties of high strength Al−Cu−Li−X aluminum-lithium alloy [J]. Rare Metal Materials and Engineering, 2007, 36(3): 493−496. (in Chinese)

[24] WANG S H, LIU C H, CHEN J H, LI X L, ZHU D H, TAO G H. Hierarchical nanostructures strengthen Al−Mg−Si alloys processed by deformation and aging [J]. Materials Science & Engineering A, 2013, 585: 233−242.

[25] HU S Y, BASKES M I, STAN M, CHEN L Q. Atomistic calculations of interfacial energies, nucleus shape and size of θ' precipitates in Al−Cu alloys [J]. Acta Materialia, 2006, 54(18): 4699−4707.

[26] VAITHYANATHAN V, WOLVERTON C, CHEN L Q. Multiscale modeling of precipitate microstructure evolution [J]. Physical Review Letters, 2002, 88(12): 1−4.

[27] VAITHYANATHAN V, WOLVERTON C, CHEN L Q. Multiscale modeling of θ' precipitation in Al−Cu binary alloys [J]. Acta Materialia, 2004, 52(10): 2973−2987.

基于时效曲线和 DSC 分析的 2519A 铝合金析出动力学

吴懿萍[1]，叶凌英[1]，贾寓真[2]，刘 玲[3]，张新明[1]

1. 中南大学 材料科学与工程学院，长沙 410083；
2. 湖南泰嘉新材料科技股份有限公司，长沙 410200；
3. 参数技术公司，上海 200120

摘 要：采用硬度测试和差示扫描量热法研究时效前不同冷轧变形量对 2519A 铝合金析出动力学的影响。根据 DSC 曲线，采用单升温速率法计算合金的激活能；采用透射电子显微镜观察冷轧和峰时效状态下合金的微观组织。结果表明：随着冷轧变形量从 7%增加至 40%，合金的时效硬化能力降低，激活能升高。当冷轧变形量为 15%时，在冷轧态合金组织中观察到密度不均匀的位错组织，在峰时效状态合金组织中观察到不均匀分布的 θ'相。不均匀分布的 θ'相可能是造成合金时效硬化能力降低和激活能升高的原因。

关键词：2519A 铝合金；位错结构；析出动力学；θ'相；差示扫描量热法

(Edited by Chao WANG)